HAL
open science

A functional analysis of speed profiles: smoothing using derivative information, curve registration, and functional boxplot

Cindie Andrieu, Guillaume Saint Pierre, Xavier Bressaud

To cite this version:

Cindie Andrieu, Guillaume Saint Pierre, Xavier Bressaud. A functional analysis of speed profiles: smoothing using derivative information, curve registration, and functional boxplot. 2013. hal-00915475v2

HAL Id: hal-00915475

https://hal.science/hal-00915475v2

Preprint submitted on 19 Jan 2014

HAL is a multi-disciplinary open access archive for the deposit and dissemination of scientific research documents, whether they are published or not. The documents may come from teaching and research institutions in France or abroad, or from public or private research centers.

L'archive ouverte pluridisciplinaire **HAL**, est destinée au dépôt et à la diffusion de documents scientifiques de niveau recherche, publiés ou non, émanant des établissements d'enseignement et de recherche français ou étrangers, des laboratoires publics ou privés.

manuscript No.
(will be inserted by the editor)

A functional analysis of speed profiles: smoothing using derivative information, curve registration, and functional boxplot

C. Andrieu · G. Saint Pierre · X. Bressaud

Abstract In this paper, we propose a functional analysis of a set of individual space-speed profiles corresponding to speed as function of the distance traveled by the vehicle from an initial point. This functional analysis begins with a functional modeling of space-speed profiles and the study of mathematical properties of these functions. Then, in a first step, a smoothing procedure based on spline smoothing is developed in order to convert the raw data into functional objets and to filter out the measurement noise as efficiently as possible. It is shown that this smoothing step leads to a complex nonparametric regression problem that needs to take into account two constraints: the use of the derivative information, and a monotonicity constraint. The performance of the proposed two-step estimator (smooth, and then monotonize) is illustrated on simulation studies and a real data example. In a second step, we use a curve registration method based on landmarks alignment in order to construct an average speed profile representative of a set of individual speed profiles. Finally, the variability of such a set is explored by the use of functional boxplots.

Keywords Functional Data Analysis · Smoothing spline · Landmarks alignment · Functional boxplots · Speed profiles

C. Andrieu
French Institute of Science and Technology for Transport, Development and Networks, Laboratory for Vehicle Infrastructure Driver Interactions (IFSTTAR/LIVIC), 77, rue des Chantiers, 78000 Versailles, France
E-mail: cindie.andrieu@ifsttar.fr

G. Saint Pierre
French Institute of Science and Technology for Transport, Development and Networks, Laboratory for Vehicle Infrastructure Driver Interactions (IFSTTAR/LIVIC), 77, rue des Chantiers, 78000 Versailles, France
E-mail: guillaume.saintpierre@ifsttar.fr

X. Bressaud
Université Paul Sabatier, Institut de Mathématiques de Toulouse, F-31062 Toulouse Cedex 9, France
E-mail: bressaud@math.univ-toulouse.fr

1 Introduction

The knowledge of the actual vehicle speeds on roads is essential from several points of view: to locate blackspot in the network, to improve the knowledge of travel time and to evaluate the effects of the modification of the infrastructure (addition of speed bumps, roundabouts, ...). The speed choice of drivers is one of the most important components of their behavior and also their road usage. This continuous information of road user's speed is available with the development of probe vehicles, that can be seen as mobile sensors exploring continuously the road network. More particularly, the development of smartphones equipped with a GPS (Global Positioning System) has increased the number of digital "traces" left by vehicles, and leads to the obtention of individual space-speed profiles that represent speed as a function of vehicle position.

The collection of individual space-speed profiles can leads to large volume of data that require the use of appropriate methods. Indeed, since in practice space-speed profiles are composed of time-stamped measurements of speed and position, most studies consider them as $\mathbb{R}^n$ vectors where n is the number of measurements. However, advances in sensors technology enable to collect data with high sampling rate that leads to high dimensional vectors (n is very large), for which classical multivariate statistical methods become inadequate because of problems related to the so-called "curse of dimensionality" and the significant correlation between close observations.

The originality of the approach presented in the current paper is to propose a functional analysis of space-speed profiles, i.e. to treat these objects as functions rather than vectors. This approach takes inspiration from Functional Data Analysis, a statistical domain that has developed considerably over the last twenty years and that appears in several domains such as meteorology, chemometrics or economics (e.g. Ramsay and Silverman 2002; Febrero et al 2007), but that is not yet widely used in road transport. Yet the functional approach is particularly suitable for the analysis of speed profiles since it allows to preserve the physical consistency between speed and position (and implicitly time), and their functional characteristics: computation of derivatives (that leads to acceleration or jerk profiles), regularity, shape constraints... An overview of the theory of statistics with functional data can be found in the monographs by Ramsay and Silverman (2002, 2005) or Ferraty and Vieu (2006), and in the reviews by Levitin et al (2007), Valderrama (2007) or more recently Cuevas (2013). Thus, after a description of a real data set composed of 78 individual space-speed profiles, we begin our analysis by a functional modeling of space-speed profiles with a definition of the corresponding functional space and the study of some mathematical properties (continuity and differentiability).

Then, the first step in the functional analysis of space-speed profiles is to convert the raw data including speed and position measurements into functional objects. It is shown that this smoothing problem can be viewed as an interesting nonparametric regression problem that needs to take into account

two constraints: the use of the derivative information, and a monotonicity constraint. In this paper, we propose a two-step estimator : smoothing step, and then monotonization step. We show that the smoothing step with the constraint of the use of the derivative information can be seen as a special case of the general spline smoothing problem (see Wahba 1990; Wang 2011) and can be solved by using the theory of reproducing kernel Hilbert spaces. Thus, the estimator proposed in this paper can be written as a linear combination of basis functions and kernel functions. However, from a computational point of view, we show that the use of a semi-kernel in place of reproducing kernel is more appropriate, and we propose to use the theory of thin-plate spline (Wahba 1990; Wahba and Wendelberger 1980) in order to obtain an estimator with a simpler form. Then, a monotonization step is proposed based on a method developed by Ramsay (1998) which has the advantage of being relatively simple to implement.

However, if this smoothing procedure leads to a set of individual space-speed profiles, when the volume of data is large, it is necessary to summarize the information contained in this set. So, in a second time, we proposed a methodology of construction of an aggregated speed profile, such as the average profile. It is then necessary to use curve registration method in order to correct phase variation (especially at stops' location), and to obtain a representative speed profile with similar features of corresponding individual speed profiles.

Finally, in a third time, we propose to apply the functional boxplot developed by Sun and Genton (2011) using an appropriate functional depth to the set of individual space-speed profiles. This graphical tool which is an extension of the classical boxplot used in the univariate setting, is very interesting to explore the variability of a functional data set. The application of this tool to speed profiles data set leads to the construction of speed corridors that reflect the variability between road users and are very informative about actual operating speed. This speed corridors are particularly adapted to driving assistance system and to enrich or update digital maps.

The remainder of the paper is structured as follows. In Sect. 2, the real data set of individual space-speed profiles used in this study is presented. In Sect. 3, we propose a definition of the functional space of space-speed profiles and we study some mathematical properties (continuity and differentiability) of these functions. In Sect. 4, we propose a two-step smoothing procedure : smooth using derivative information, and then monotonize. Performance and limitations of the estimator are discussed on simulation studies and the real data set. In Sect. 5, we propose a methodology of construction of an average speed profile using a curve registration procedure based on the method of landmarks alignment. In Sect. 6, we apply the functional boxplot to the real data set of individual speed-profiles and show the interest of these speed corridors to explore the variability between road users. Finally, Sect. 7 provides the main conclusions of the present study.

2 The data

We consider in this paper a data set extracted from an experiment conducted by the French laboratory IFSTTAR-LIVIC and that took place in 2012 in Versailles, France. Thirty-nine drivers participated to this experiment and performed twice a road section of urban and inter-urban type with a length of about 1100 m. This road section, illustrated at Fig. 1, corresponds to the path from A to B and is composed of a stop sign, two roundabouts and a traffic light. For logistical reasons, two vehicles were used for this experiment: a Renault Clio III equipped with a Garmin GPS 16x LVC (for 20 drivers), and a Renault Modus with a GPS GlobalSat BR-355 (for 19 drivers). Note that the use of two vehicles and the fact that each driver performed twice the studied section lead to conditions close to naturalistic driving studies where different drivers were observed in a natural setting, in particular during regular travels such as the commute to work. Thus, we do not take into account the correlation between the two paths of the same driver.

Fig. 1 Map of the studied section.

The data-logger collects vehicle position (latitude and longitude) and speed via GPS at a 1Hz sampling frequency (i.e. 1mes/sec). Note that GPS receivers use the Doppler shifts of the satellite signals to calculate vehicle speed, which implies that vehicle speed is independent of vehicle position. In order to reduce the GPS position measurements to a one-dimensional framework, it is assumed that these are map-matched, so that the vehicle is positioned on the correct road segment. Many map-matching algorithms have been developed to identify the correct road segment on which the vehicle is travelling. Thus, in this paper, GPS measurements represent the curvilinear abscissa of the vehicle on the studied road segment (absolute location) from the initial position (point A).

The aim of the study is to focus on space-speed profiles from this data set, i.e. speed as a function of the distance traveled by the vehicle from the point A. Since the 39 drivers performed twice the studied section, the data set is composed of 78 individual space-speed profiles illustrated at Fig. 2.

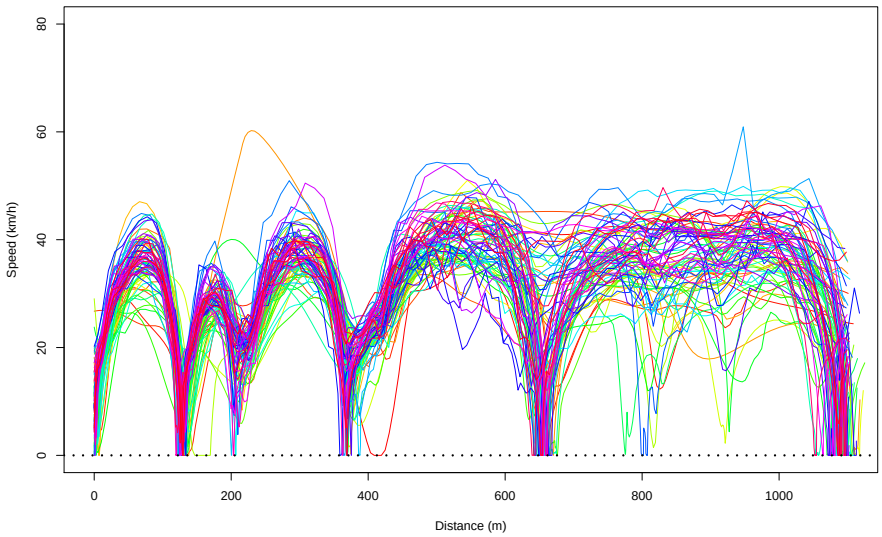

Fig. 2 Sample of 78 space-speed profiles : raw data.

3 Functional modeling of space-speed profiles

3.1 Definition of space-speed profiles

Before beginning a functional analysis of space-speed profiles, it is necessary to define the functional space of such objects. Indeed, any function $f : \mathbb{R}^+ \longrightarrow \mathbb{R}^+$ is not a space-speed profile (e.g. a constant function equal to zero). In practice, a space-speed profile is a sequence of time-stamped measurements of position (from GPS or odometer) and speed, so it can be studied in the three following study areas: `distance` $\times$ `time`, `speed` $\times$ `time` and `speed` $\times$ `distance` (see Fig. 3).

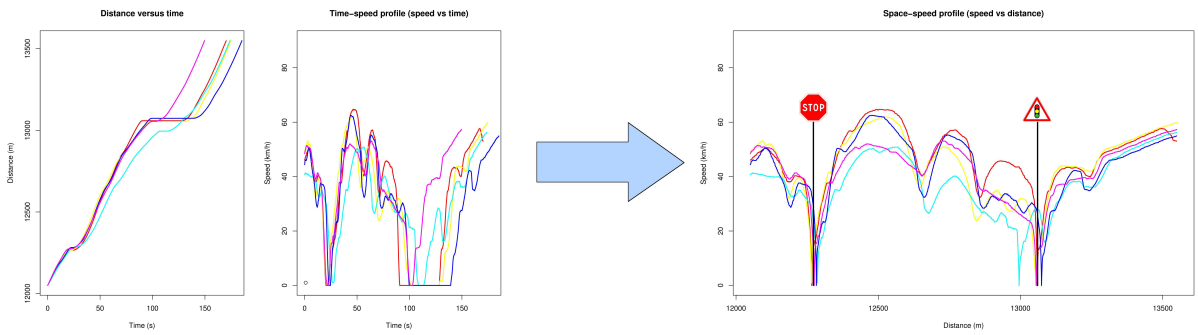

Fig. 3 Link between the three study areas : [`distance` $\times$ `time`, `speed` $\times$ `time`] and [`speed` $\times$ `distance`].

The functions defined in each of these three study areas are related mathematically: if we denote $F(t)$ a function defined in the study area `distance` $\times$ `time` that represents the distance traveled as function of time, the derivative function $F'(t)$ represents the speed as function of time and is defined in the study area `speed` $\times$ `time`. So, by definition, the function F must be increasing and at least of class $\mathcal{C}^1$. In order to define an acceleration profile, we propose to require that F is at least $\mathcal{C}^2$, and so we propose the following definition of the functional space of space-speed profiles :

Definition 1 Let $x_f \in \mathbb{R}^+$. Then the space of space-speed profiles, denoted $\mathcal{E}_{SSP}$, is defined as follows :
$\mathcal{E}_{SSP} = \{v_S : [0, x_f] \longrightarrow \mathbb{R}^+$ such that there exists a positive real T and an increasing function $F : [0, T] \longrightarrow [0, x_f]$ of class $\mathcal{C}^2$ with $F(0) = 0$ such that $v_S(x) = F' \circ F^{-1}(x)), x \in [0, x_f]\}$,
where F^{-1} is the generalized inverse of F defined by $F^{-1}(x) = inf\{t \in [0, T], F(t) = x\}$.

The positive real numbers x_f and T represent respectively the length and the travel time of the studied section. Fig. 4 illustrates Definition 1 by showing the functional link between distance, speed and implicitly time.

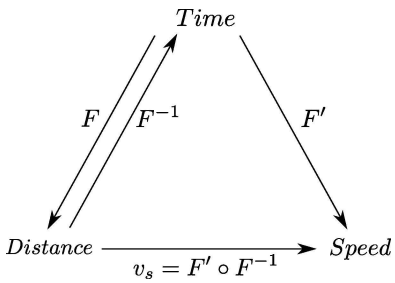

Fig. 4 Functional diagram illustrating the definition of space-speed profiles.

3.2 Mathematical properties of space-speed profiles

We studied some properties of the space-speed profiles, i.e. functions in the space $\mathcal{E}_{SSP}$ (as defined in Definition 1). The continuity property is given by the following theorem whose proof is deferred to Appendix A:

Theorem 1 *All functions $v_S : [0, x_f] \longrightarrow \mathbb{R}^+$ belonging to the space of space-speed profiles $\mathcal{E}_{SSP}$ (as defined in Definition 1) are continuous on $[0, x_f]$.*

If the continuity property of space-speed profiles is obvious, the differentiability property is less intuitive as shown in the following theorem whose proof is also deferred to Appendix A:

Theorem 2 *Assume that $v_S : [0, x_f] \longrightarrow \mathbb{R}^+$ belongs to the space of space-speed profiles $\mathcal{E}_{SSP}$ (as defined in Definition 1). Let $H_0 = \{x \in [0, x_f], v_S(x) = 0\}$, all points for which the speed is zero. The two following assumptions are added:*

- (H_1) *Assume that F is of class $\mathcal{C}^2$ on $[0, T]$ and strictly increasing, and $\exists t_0 \in]0, T[$ such that $F'(t_0) = 0$ and $F'''(t_0)$ exists with $F'''(t_0) \neq 0$.*
- (H_2) *Assume that F is of class $\mathcal{C}^2$ on $[0, T]$ and increasing, $\exists t_0, t_1 \in]0, T[$, $t_0 \neq t_1$ such that $F'(t) = 0$ on $[t_0, t_1]$, and the function G defined on $[0, T-(t_1-t_0)]$ by:*

$$\begin{cases} \text{for } t \leq t_0, & G(t) = F(t), \\ \text{for } t \geq t_0, & G(t) = F(t + t_1 - t_0), \end{cases}$$

  satisfies the assumptions (H_1).

If F satisfies the assumptions (H_1) or (H_2), then $v_S = F' \circ F^{-1}$ is not differentiable on H_0.

The assumptions (H_1) and (H_2) are not restrictive and are satisfied in most cases. So, this theorem shows that space-speed profiles are not differentiable at points for which the speed is zero, i.e. when the vehicle is stopped. From a geometrical point of view, if we assume that $x_0 \in H_0$ (i.e. $v_S(x_0) = 0$), it is easily shown that the graph of a space-speed profile v_S has a half-tangent parallel to the axis of y in x_0, i.e. a cusp at the point $(x_0, 0)$.

This property of non differentiability at points for which the speed is zero, implies some difficulties in the calculation of an average profile, particularly in the case of stops. Indeed, if a space-speed profile v_1 is equal to zero at a point x_0, and a space-speed profile v_2 is strictly positive at x_0, then the sum $v_1 + v_2$ is not a space-speed profile as defined in the Definition 1 since $v_1 + v_2$ is not differentiable at x_0 but $(v_1 + v_2)(x_0) > 0$. Thus, the calculation of an average profile is meaningful only in this two cases:

- when all space-speed profiles are strictly positive (no stops) ;
- when all space-speed profiles are equal to zero at the same points (i.e. all vehicles stop at the same location).

This second case raises the issue of registration of speed profiles that will be discussed in Sect. 5.

4 Estimation of a space-speed profile from noisy data: A smoothing problem under constraints

The first step of a functional analysis is to convert the raw data into functional objects that leads to the use of an adapted smoothing procedure. However, the estimation of a space-speed profile from noisy measurements of position and speed is a complex nonparametric regression problem (see for example Andrieu et al 2013). Indeed, on the one hand, both the response variable (corresponding to speed) and the explanatory variable (corresponding to vehicle position) are noisy. And on the other hand, the regression function must belong to the space $\mathcal{E}_{SSP}$ defined in Definition 1 and then check its properties, in particular the non differentiability when the speed is zero. To overcome these difficulties, we propose to change to a more suitable study area and start by estimating the function F representing the distance traveled as function of time (study area `distance` $\times$ `time` in Fig. 3). Then the new nonparametric model is

$$y_i = F(t_i) + \varepsilon_{x,i}, \quad i = 1, \ldots, n, \tag{1}$$

where y_i are noisy observations of the distance traveled, $\varepsilon_{x,i}$ are uncorrelated errors with zero mean and σ_x^2 variance, and $F(t)$ is the regression function. This change of study area leads to take into account the two following constraints:

1. Use the derivative information, i.e. estimate the regression function $F(t)$ of the model (1) from both noisy observations of F corresponding to position measurements, and noisy observations of its derivative F' corresponding to speed measurements.
2. A monotonicity constraint since the function F representing the distance traveled as function of time must be increasing.

The consideration of these two constraints in the smoothing step is the subject of the two following subsections. Then, once we have obtained an estimator $\widehat{F}$ of the function F, it is easy to deduce by differentiation an estimator $\widehat{F}'$ of the time-speed profile, and finally to deduce an estimator $\widehat{v}_S$ of the space-speed profile v_S by the transformation $\widehat{v_S} = \widehat{F}' \circ \widehat{F}^{-1}$.

4.1 Smoothing using derivative information

The first constraint in the nonparametric model (1) is to use the derivative information, i.e. to estimate the regression function $F(t)$ from both noisy measurements of position and speed. Assume that the domain of $F(t)$ is $\mathcal{X} = [0, T]$, where T is a positive real, and $F \in W^m[0, T]$ where $W^m[0, T]$ is the Sobolev space of order m with $m > 1$. Then the use of the derivative information leads to consider the following data model:

$$\begin{cases} y_i = F(t_i) + \varepsilon_{x,i}, & i = 1, \ldots, n \\ v_i = F'(t_i) + \varepsilon_{v,i}, & i = 1, \ldots, n \end{cases} \tag{2}$$

where y_i and v_i are noisy measurements of distance traveled and speed respectively at each sampling time t_i, and $\varepsilon_{x,i}$ and $\varepsilon_{v,i}$ are independent zero mean errors with variance σ_x^2 and σ_v^2 respectively. We also assume that for all $i = 1, \ldots, n$, $\varepsilon_{x,i}$ and $\varepsilon_{v,i}$ are independent. Note that we have assumed that the observations y_i and v_i are obtained at the same times t_i. Otherwise, a data resampling will lead to this case.

The problem of smoothing with derivative information appears in various applications such as economy (Hall and Yatchew 2007), molecular biology (Calderon et al 2010) or image analysis (Mardia et al 1996). We propose to solve this problem by using smoothing splines, which have the advantage of requiring the estimation of a single smoothing parameter λ, contrary to penalized splines used by Calderon et al (2010), for which the choice of the number of knots can be difficult. Thus, this problem can be seen as a special case of the general spline smoothing problem (see Wahba 1990; Wang 2011) and can be solved by using the theory of reproducing kernel Hilbert spaces (see Cox 1988). Then, the estimator can be written as a linear combination of basis functions and kernel functions. However, to compute the estimator, it is necessary to choose a norm associated with the design space (in this study, the Sobolev space $W^m[0, T]$) that is suitable. Indeed, the expression of the reproducing kernels used for calculating the estimator depends on the choice of this norm, and can leads to difficulties in the numerical computation (see Berlinet and Thomas-Agnan 2004 for a collection of examples of spaces, norms, and kernels, and Andrieu 2013, Chap. 4 for more details). So, we propose to use the theory of thin-plate spline which leads to similar results for the form of the estimator (see Duchon 1977; Meinguet 1979; Wahba and Wendelberger 1980), but where the reproducing kernel is replaced by a semi-kernel with a simpler form that greatly simplifies the computation of the estimator.

The model (2) is a particular case of the general spline smoothing model defined in Wahba (1990), since it can be rewritten as follows:

$$y_j = \mathcal{L}_j F + \varepsilon_j \ , \quad j = 1, \ldots, 2n, \tag{3}$$

where

– the observations y_j are defined by:
$$\begin{cases} y_j = y_i \ \text{ with } \ i = j \ \text{ for } \ j = 1, \ldots, n \\ y_j = v_i \ \text{ with } \ i = j - n \ \text{ for } \ j = n+1, \ldots, 2n \end{cases},$$

– the bounded linear functionals $\mathcal{L}_j$ on $W^m[0,T]$ are defined by:
$$\begin{cases} \mathcal{L}_j F = F(t_i) \ \text{ with } \ i = j \ \text{ for } \ j = 1, \ldots, n \\ \mathcal{L}_j F = F'(t_i) \ \text{ with } \ i = j - n \ \text{ for } \ j = n+1, \ldots, 2n \end{cases},$$

– the errors ε_j are defined by:
$$\begin{cases} \varepsilon_j = \varepsilon_{x,i} \ \text{ avec } \ i = j \ \text{ pour } \ j = 1, \ldots, n \\ \varepsilon_j = \varepsilon_{v,i} \ \text{ avec } \ i = j - n \ \text{ pour } \ j = n+1, \ldots, 2n \end{cases}.$$

A useful result state that the operator L defined by $Lf = \frac{\partial^k f}{\partial^{\alpha_1} x_1 \ldots \partial^{\alpha_d} x_d}$ for $\alpha_1 + \ldots + \alpha_d = k$ $(k, \alpha_1, \ldots, \alpha_d \in \mathbb{N})$ is a continuous linear form if and only if $2m - 2k - d > 0$ (see Berlinet and Thomas-Agnan 2004, Th. 133; Wahba and Wendelberger 1980). So, we can deduce that linear functionals in the model (3) are bounded on $W^m[0,T]$ if $m > 1$ since $d = 1$, $k = 0$ for $j = 1, \ldots, n$ and $k = 1$ for $j = n+1, \ldots, 2n$. Then, an estimator of $F(t)$ is the minimizer of the following penalized least squares criterion in $W^m[0,T]$:

$$\frac{1}{2n}\{\sigma_x^{-2} \sum_{i=1}^{n} (y_i - F(t_i))^2 + \sigma_v^{-2} \sum_{i=1}^{n} (v_i - F'(t_i))^2\} + \lambda \int_0^T (F^{(m)}(t))^2 dt. \quad (4)$$

A solution to a more general minimization problem extended to dimension $d \geq 1$ of which the minimization problem (4) is a special case with $d = 1$, is given in Wahba and Wendelberger (1980). Before stating the result, we introduce the m polynomials functions $\phi_1, \ldots, \phi_m$ as a basis of the null space of the penalty functional $J_m(f) = \int_0^T (f^{(m)}(t))^2 dt$, i.e. $\mathcal{H}_0 = \{f : J_m(f) = 0\}$. Thus, provided that the two hypothesis on the linear functionals ($L_1, \ldots, L_n$ linearly independent continuous linear functionals, and $L_k \sum_{\nu=1}^{p} a_\nu \phi_\nu = 0$ implies that all the a_ν are 0) are satisfied, which it's the case if the sampling points $t_1, \ldots, t_n$ are distincts, we can deduce that the minimizer of (4) can be written as:

$$\widehat{F}_\lambda(t) = \sum_{\nu=1}^{m} d_\nu \phi_\nu(t) + \sum_{i=1}^{n} c_i E_m(t_i, t) + \sum_{i=1}^{n} c_i' \frac{\partial}{\partial s} E_m(s,t)|_{s=t_i}, \quad (5)$$

where

$$E_m(s,t) = \theta_{m,1} |s - t|^{2m-1},$$
$$\theta_{m,1} = \frac{\Gamma(1/2 - m)}{2^{2m} \pi^{1/2} (m-1)!}.$$

The coefficients $c = (c_1, \ldots, c_n, c_1', \ldots, c_n')^T$ and $d = (d_1, \ldots, d_m)^T$ are solutions of the linear system

$$(K + n\lambda W^{-1})c + Td = y, \quad (6)$$
$$T^T c = 0, \quad (7)$$

where

$$T = \{\mathcal{L}_j \phi_\nu\}_{j=1}^{2n}{}_{\nu=1}^{m},$$
$$K = \{\mathcal{L}_{j(s)} \mathcal{L}_{k(t)} E_m(s,t)\}_{j,k=1}^{2n},$$
$$W = diag(\sigma_x^{-2}, \ldots, \sigma_x^{-2}, \sigma_v^{-2}, \ldots, \sigma_v^{-2}).$$

The solution $\widehat{F}_\lambda(t)$ is then a polynomial spline of order m with knots at the sampling time $t_1, \ldots, t_n$. Note that the bivariate function $E_m(s,t)$, called semi-kernel, acts like a reproducing kernel in this approach, but its simple form is more appropriate for computational aspect and specifically for solving the linear system defined by Eqs. (6) and (7).

The error variances σ_x^2 and σ_v^2 are usually unknown in practice. In general, we use an estimator of the error variance corresponding to the criterion used for the selection of the smoothing parameter λ. Three scores are commonly used:

- the UBR score ("Unbiased Risk") which is an extension of the Mallow's C_p criterion ;
- the GCV score ("Generalized Cross-Validation") which is a weighted version of the standard cross-validation ;
- the GML score ("Generalized Maximum Likelihood") based on a Bayesian model, and that required a normality assumption on the errors.

The selection of the smoothing parameter results from the minimization of one of these criteria, and the error variances estimates depend on the smoothing parameter obtained, and therefore on the criterion chosen (see Gu 2002). Thus, if in a first time, we consider only the position measurements, i.e. the data model (1), and if we denote $A(\lambda)$ the hat matrix defined by

$$(\widehat{F}_\lambda(t_1), \ldots, \widehat{F}_\lambda(t_n))^T = A(\lambda)y, \tag{8}$$

where $\widehat{F}_\lambda$ is the smoothing spline estimate of F for the smoothing parameter λ (that is a polynomial spline of order $2m$), then the variance estimate of σ_x^2 associated with the GCV criterion is

$$\widehat{\sigma}_{gcv}^2 = \frac{y^T(I - A(\lambda_v))^2 y}{tr(I - A(\lambda_v))}, \tag{9}$$

and the variance estimate associated with the GLM criterion is

$$\widehat{\sigma}_{gml}^2 = \frac{y^T(I - A(\lambda_m))y}{n - m}. \tag{10}$$

Similarly, in a second time, we consider only the speed measurements and calculate the smoothing spline estimate of F' for the smoothing parameter λ, and then deduce an estimate of the variance error σ_v^2.

4.2 Smoothing under monotonicity constraint

The second constraint in the nonparametric model (1) is a monotonicity constraint since the function F representing the distance traveled as a function of time must be increasing. Various methods of smoothing under monotonicity constraint have been developed. The main approaches are based on kernel smoothers and splines. An overview of these methods can be found in Delecroix and Thomas-Agnan (2000). Among the main methods, we can cite the isotonic regression introduced by Brunk (1955), the monotone splines (for example, Ramsay introduces the I-splines basis in Ramsay 1988 for monotone regression splines) or the projection methods (e.g. Delecroix et al 1996 or Mammen et al 2001).

In a previous study (Andrieu et al 2012), the method of homeomorphic splines developed by Bigot and Gadat (2010) have been tested. However, if the monotonization step presented good results, we had difficulties in the implementation of the derivative. So, we propose to use a method developed by Ramsay (1998) which has the advantage of being relatively simple to implement. The principle of this method is to transform the constrained smoothing problem to an unconstrained one. A monotone function has a positive first derivative. So the main idea is that any strictly monotonic function f satisfies the following differential equation:

$$D^2 f = wDf, \tag{11}$$

where Df and $D^2 f$ are respectively the first and second derivative of the function f, and w is an unconstrained function. Thus, any strictly monotonic function f can be written as following (as solution of the Eq. (11)):

$$f(t) = \beta_0 + \beta_1 \int_0^t exp[\int_0^u w(v)dv]du, \tag{12}$$

where β_0 and β_1 are arbitrary constants such that $f(0) = \beta_0$ and $f'(0) = \beta_1$. Then, the problem is to estimate the coefficients β_0 and β_1 and the unconstrained function w by minimizing the following criterion:

$$\sum_{i=1}^{n} (y_i - \beta_0 - \beta_1 h(t_i))^2 + \lambda \int_0^T (w^m(t))^2 dt, \tag{13}$$

where

$$h(t) = \int_0^t exp[\int_0^v w(v)dv]du. \tag{14}$$

The unconstrained function w is computed using an appropriate basis expansion (e.g. B-splines) and the coefficients β_0 and β_1 are estimated by numerical algorithms. However, due to a numerical optimization of the criterion (13), monotone smoothing spline involves considerably more computation than the usual smoothing spline process.

Thus, the monotonicity constraint is consider in a second smoothing step by applying the method of Ramsay described above, to the estimated values $\widehat{F}_\lambda(t_i)$ obtained at the first smoothing step for which we have used the speed measurements (Section 4.1). Therefore, this second smoothing step can be seen as a monotonization step and then is similar to the projection step in projection methods (see Mammen et al 2001). The new monotone estimator of $F(t)$ is then denoted $\widehat{F}_{mc}$ (with "mc" for monotonicity constraint), and finally we deduce an estimator $\widehat{v}_S$ of the space-speed profile v_S by the transformation $\widehat{v_S} = \widehat{F}'_{mc} \circ \widehat{F}^{-1}_{mc}$.

4.3 Simulation study

We propose to illustrate the performance of our smoothing procedure on three simulated examples. For each example, we study the monotone estimator $\widehat{F}_{mc}$ obtained after the two steps of the smoothing procedure (use of derivative information, and then monotonization), the derivative $\widehat{F}'_{mc}$ of this estimator, and the composite function $\widehat{F}'_{mc} \circ \widehat{F}^{-1}_{mc}$.

We investigate the regression model (2) with a fixed design made up of $n = 50$ points evenly distributed on $[0, 1]$ for the first and second example, and $n = 150$ points evenly distributed on $[0, 3]$ for the third example. The errors term $\varepsilon_{x,i}$ and $\varepsilon_{v,i}$ were simulated from centered gaussian distributions with $\sigma_x = 0.2$ and $\sigma_v = 0.01$. This choice of a smaller noise for the derivative of F than for F is motivated by the fact that speed measurements are generally more accurate than position measurements. The increasing regression functions chosen in these three examples are:

$$F_1(t) = t^2 \quad \text{with} \quad t \in [0, 1], \tag{15}$$

$$F_2(t) = \frac{1}{2}(2t-1)^3 + \frac{1}{2} \quad \text{with} \quad t \in [0, 1], \tag{16}$$

$$F_3(t) = \begin{cases} (t-1)^3 + 1 & \text{si } t \leq 1 \\ 1 & \text{si } 1 \leq t \leq 2 \\ (t-2)^3 + 1 & \text{si } t \geq 2 \end{cases} \quad \text{with} \quad t \in [0, 3], \tag{17}$$

and correspond respectively to a convex function, a function with a small plateau (inflection point), and a function with a large plateau (F_3 is an extension of F_2 with a plateau over $[1, 2]$). The different functions, their derivatives, and the composite functions $F'_i \circ F_i^{-1}$, $i = 1, 2, 3$, are displayed Fig. 5 (dashed blue lines).

The proposed estimator $\widehat{F}_{mc}$ of the the unknown regression function F for the three examples (15)-(17) is the solid red line (left column in Fig. 5). As described in the previous section, this estimator was calculated in two steps. The first step corresponding to the construction of the estimator (5) that take into account the derivative information, was computed with the function `ssr` in the R (R Core Team 2013) package `assist` (Wang and Ke 2004). In the three examples, we have chosen $m = 3$ (i.e. a quintic spline) for the order of

the Sobolev space, and the GML criterion was used for the selection of the smoothing parameter. The second step corresponding to the monotonization of the estimator (5) was computed with the function `smooth.monotone` in the R package `fda`. We have chosen $m = 3$ for the degree of the penalty in Eq. (13), and the smoothing parameter was chosen by trial and error.

The derivative $\widehat{F}'_{mc}$ of the estimator is represented in the middle column of the Fig. 5, and the composite function $\widehat{F}'_{mc} \circ \widehat{F}^{-1}_{mc}$ is in the right column (red lines). The computation of a point $t_0 = F^{-1}(y_0)$ was made by the computation of the root (i.e. zero) of the function $F(t) - y_0$ (use of the R function `uniroot`). Due to computational problems of the inverse function at the edge of the interval, the composite function $F' \circ F^{-1}$ and its estimator was computed over [0.1,0.9] for the first and second example (15)-(16), and over [0.1,1.9] for the third example (17).

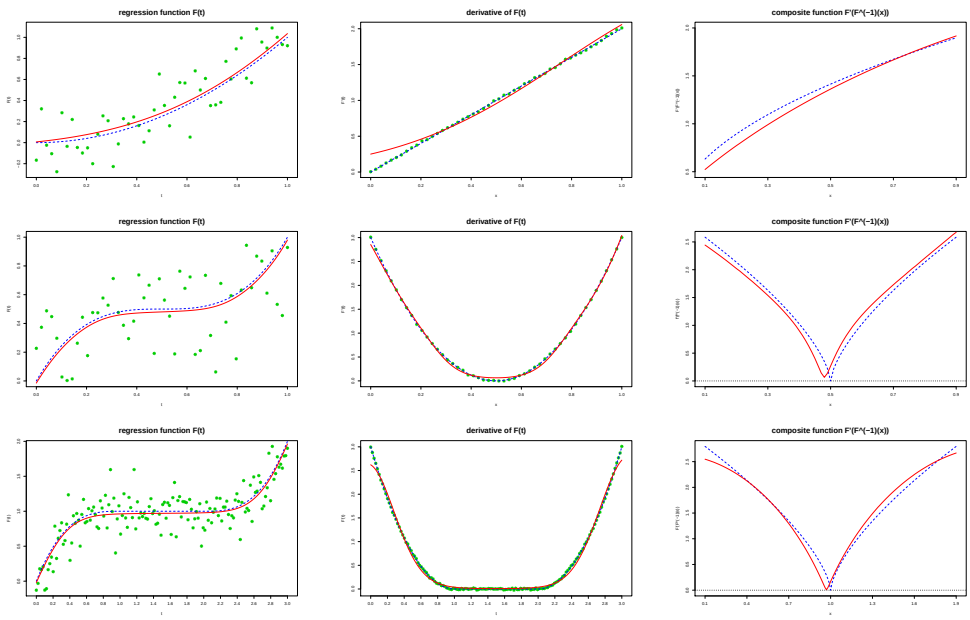

Fig. 5 Estimators of F, F' and $F' \circ F^{-1}$ (left to right) for the three examples (15)-(17) (top to bottom). The unknown regression function F, its derivative F' and the composite function $F' \circ F^{-1}$ are dashed blue lines. The noisy data are green points. The estimators $\widehat{F}_{mc}$, $\widehat{F}'_{mc}$ and $\widehat{F}'_{mc} \circ \widehat{F}^{-1}_{mc}$ are solid red lines.

We use 100 simulation runs to calculate the pointwise mean squared error (MSE) for the estimators $\widehat{F}_{mc}$ and $\widehat{F}'_{mc}$ evaluated on an equidistant grid of size $2n$, and for the estimator $\widehat{F}'_{mc} \circ \widehat{F}^{-1}_{mc}$ evaluated on an equidistant grid with a step equal to 0.01. Curve of these MSE for the three examples are displayed

Fig. 6. Table 1 shows the results of the mean integrated squared error (MISE) for the estimators $\widehat{F}_{mc}$, $\widehat{F}'_{mc}$ and $\widehat{F}'_{mc} \circ \widehat{F}^{-1}_{mc}$ in the three examples.

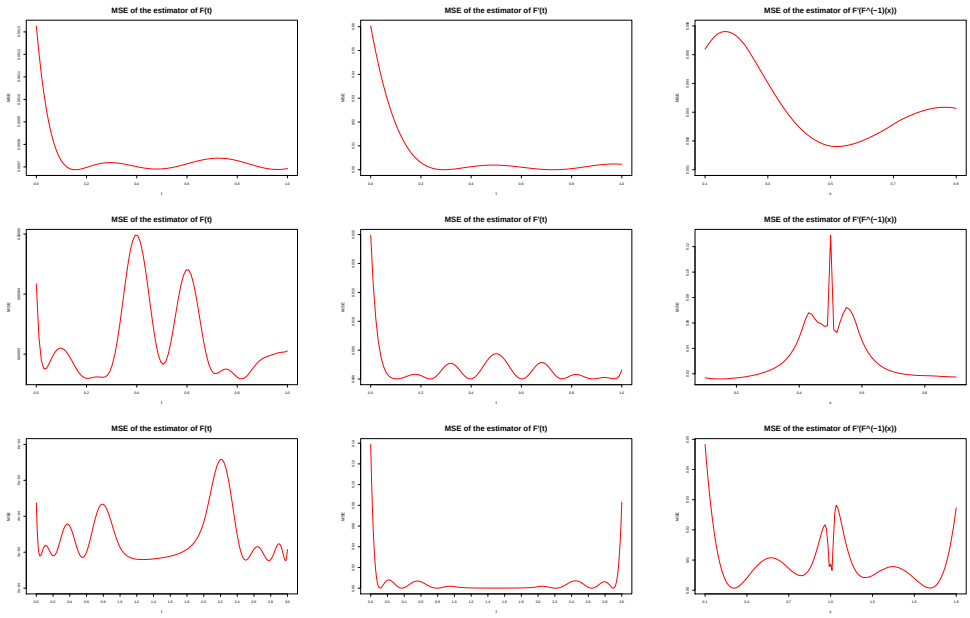

Fig. 6 Simulated mean squared error of the estimators $\widehat{F}_{mc}$, $\widehat{F}'_{mc}$ and $\widehat{F}'_{mc} \circ \widehat{F}^{-1}_{mc}$ (left to right) computed over 100 simulations runs on the three examples (15)-(17) (top to bottom).

Table 1 Mean integrated squared error (MISE) of the estimators $\widehat{F}_{mc}$, $\widehat{F}'_{mc}$ and $\widehat{F}'_{mc} \circ \widehat{F}^{-1}_{mc}$, over the 100 simulations for each example.

	$\widehat{F}_{mc}$	$\widehat{F}'_{mc}$	$\widehat{F}'_{mc} \circ \widehat{F}^{-1}_{mc}$
function F_1	0.00074	0.0059	0.0033
function F_2	0.00084	0.0017	0.033
function F_3	0.00034	0.0044	0.0092

Fig. 5 and Fig. 6 show the good results of the estimators $\widehat{F}_{mc}$, $\widehat{F}'_{mc}$ and $\widehat{F}'_{mc} \circ \widehat{F}^{-1}_{mc}$, even if we observe some boundary effects at the edge of the interval especially for the derivative estimator $\widehat{F}'_{mc}$. As mentioned Sect. 3.2, the difficulty in the estimation of the composite function $F' \circ F^{-1}$ is the estimation of the cusp when the function is equal to zero, and that corresponds to a plateau for the function F. The comparison between results obtained with the example

(16) (regression function F_2 with a small plateau) and the example (17) (regression function F_3 with a large plateau) shows that the cusp is overestimate in the case of a small plateau (in the example (16), the estimator $\widehat{F}'_{mc} \circ \widehat{F}^{-1}_{mc}$ does not cross the axis). This problem results from the mononization step, since the method of Ramsay which is used, provides a strictly increasing estimator $\widehat{F}_{mc}$ that is not appropriate for the estimation of plateaux even if in practice only small plateaux are not very good estimated. However, actually, we have not found a solution for this problem.

4.4 Application to the real data example

To illustrate the performance of the smoothing procedure in the estimation of space-speed profiles from noisy position and speed measurements, we applied the method on the real data set presented in Sect. 2. Thus, the smoothing procedure is applied to the data set of 78 individual space-speed profiles illustrated at Fig. 2 and reproduced Fig. 7.a, that are composed of noisy position and speed measurements, as follows:

1. A first smoothing step using derivative information, with for each path j, $j = 1, \ldots, 78$, an estimation $\widehat{F}_{\lambda_j}(t)$ of each function $F_j(t)$ (representing the distance traveled as function of time) with the following parameters:
   - an estimation of the variance $\sigma^2_{x,j}$ and $\sigma^2_{v,j}$ for each path j, $j = 1, \ldots, 78$;
   - $m = 3$ (quintic spline);
   - an automatic selection of each smoothing parameter λ_j resulting from the minimization of the GML criterion.
2. A second smoothing step under monotonicity constraint, corresponding to a monotonization of each estimate $\widehat{F}_{\lambda_j}(t)$ obtained at the previous step with the following parameters:
   - $m = 3$ for the degree of the penalty ;
   - a selection of each smoothing parameter by trial and errors.

Fig. 7.b illustrates the results of this smoothing procedure and shows the smooth individual space-speed profiles obtained with the transformation $\widehat{F}'_{j,mc}(t) \circ \widehat{F}^{-1}_{j,mc}(t)$. Results are good since some peaks which appear in raw data, and that probably correspond to outliers, are reduced (e.g. blue and orange curves). Missing values are also be corrected by the smoothing procedure. The disadvantage of the step monotonisation mentioned in the simulation study, which causes an over-estimation of speed, appears mainly at the stop sign (short stop) but is less important at the traffic light (long stop). Finally, note that the main difference between Fig. 7.a and Fig. 7.b is that the smoothing procedure allows to reduce the study of these individual speed profiles to a functional framework since the estimated space-speed profiles belong to the space $\mathcal{E}_{SSP}$ defined in Definition 1. Some advantages of studying a set of individual space-speed profiles in a functional framework are illustrated in the next sections.

a. Raw data.

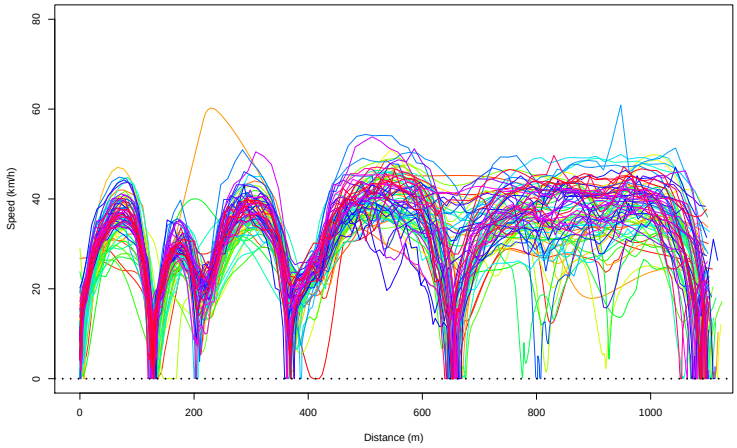

b. Smooth data.

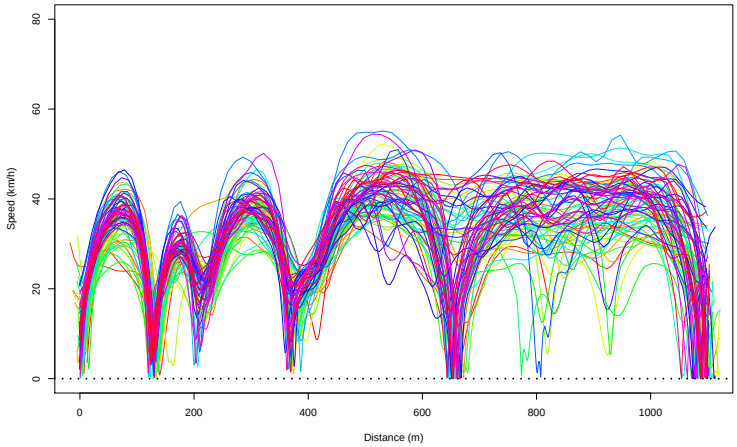

Fig. 7 Smoothing step on the 78 individual space-speed profiles.

5 Curve registration by landmarks alignment

The second step of our analysis is to summarize the information contained in a data set of individual space-speed profiles by the construction of the average profile. However, due to phase variation (i.e. horizontal variation) between the individual speed profiles, especially at stops (all vehicles do not stop at the same location), it is necessary to align them in order to obtain an aggregated profile which is representative of the set.

The *curve registration* or *curve alignment* problem appears in many areas such as biology, meteorology, pattern recognition... (Ramsay and Li 1998; Bigot 2006). Indeed, frequently, observed curves exhibit two types of variability: *amplitude variation* which corresponds to vertical variation, and *phase variation* which corresponds to horizontal variation (Ramsay and Silverman 2005). Then, to build a representative curve of a set of observed curves, it is necessary to correct the phase variation in order to obtain curves with similar features. The curve registration problem consists in finding, for each curve, a warping function and to deform all the curves in order to align them. If the literature about this problem is relatively large (e.g. Kneip and Gasser 1992; Wang and Gasser 1997), it is not treated or treated in a simple way in velocity profiles studies.

We propose to use the method of landmarks alignment which consists to determine, for each curve, a deformation function so that specific points called landmarks of the registered curves are aligned. Specific points defined as landmarks are generally the positions of maxima, minima, inflection points, or zero crossings. Then, the landmarks registration of m signals $f_1, \ldots, f_m$ defined on the same interval $[0, X]$ can be divided into the five following steps:

1. Definition of characteristic points to be used as landmarks (eg, minimum, maximum, zero crossing ...).
2. Extraction of landmarks $x_{i,1}, \ldots, x_{i,K}$ from an observed sequence of each signal f_i, $i = 1 \ldots, m$. Note that since observed signals are noisy, the landmarks $x_{i,1}, \ldots, x_{i,K}$ are usually extracted from a estimator $\widehat{f_i}$ of the signal f_i.
3. Identify landmarks reference $x_{0,1}, \ldots, x_{0,K}$, i.e. the points at which the curves must match.
4. Determine deformation functions $h_1, \ldots, h_m$ so that corresponding landmarks are matched, i.e. for all $i = 1, \ldots, m$, $h_i(x_{0,j}) = x_{i,j}$, $j = 1, \ldots, K$.
5. Deformation of the signals using transformations obtained in the previous step. The registered functions $\widetilde{f_i}(x) = f_i[h_i^{-1}(x)]$, $i = 1, \ldots, m$, are then aligned at each points $x_{0,1}, \ldots, x_{0,K}$.

The deformation functions $h_i(x)$, $i = 1 \ldots, m$, called *warping functions*, must check the following properties:

- Initial conditions: $h_i(0) = 0$, $h_i(X) = X$.
- Landmarks alignment: $h_i(x_{0,j}) = x_{i,j}$.
- Strict monotonicity: $x_1 < x_2$ implies $h_i(x_1) < h_i(x_2)$ (in order to respect the sequencing of points).

The method of landmarks alignment is applied to the set of speed profiles illustrated at Fig. 7.b. In order to compare similar speed profiles, we distinguish the two driving situations corresponding to the state of the traffic light (red or green light). Only the red light case will be studied in the following, that represents a sample of 36 individual profiles. We have chosen to define

a. Unregistered space-speed profiles.

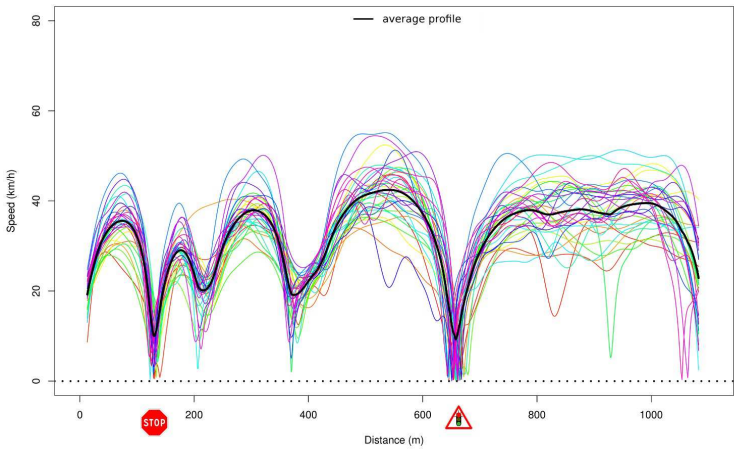

b. Registered space-speed profiles.

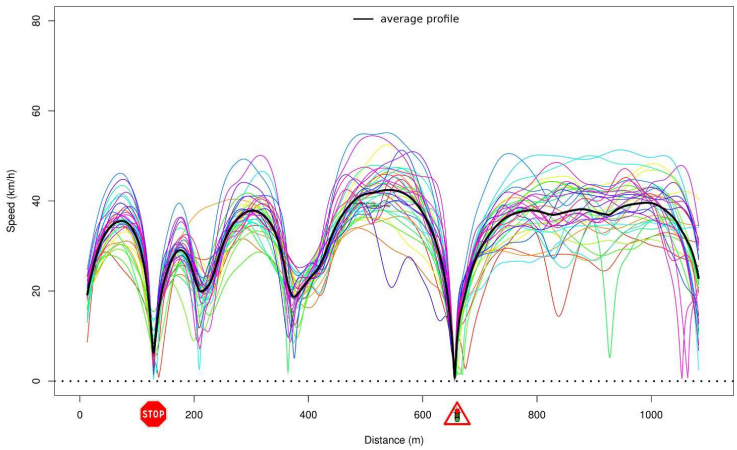

Fig. 8 Registration of space-speed profiles in the red light case (36 curves). The black curve is the average profile.

landmarks as the positions of the two elements of the infrastructure that require a stop of the vehicle, namely the stop sign and the red light. Thus, the landmarks, corresponding to zero-crossing (or local minima) at the stop sign and the traffic light positions, are extracted from the estimated space-speed profiles obtained with the smoothing procedure, and are matched with the reference landmarks defined by the average position of vehicle stops at this two elements of the infrastructure. Then, monotone cubic spline interpolation have been determined as warping functions and have been computed with the R function `splinefun` and the option "monoH.FC". We also impose the condition that the warping functions are linear with a slope equal to one around the stops (we fix an interval of length 100 m around each stop) in order to not

too distort the space-speed profiles in the neighborhood of each stop and to obtain "true" space-speed profiles as defined in Definition 1.

Fig. 8 compares the unregistered (Fig. 8.a) and the registered (Fig. 8.b) speed profiles in the red light case (36 curves). Fig. 8.a illustrates the fact that averaging unregistered profile results in an average profile (black curve) that is not representative of the set of the individual speed profiles. Indeed, this average profile doesn't equal to zero at the red light unlike all individual profiles. In contrast, Fig. 8.b shows that the average of the registered profiles tends to resemble much more closely most of the individual profiles, and then is a good aggregated speed profile of the sample.

6 Functional boxplot: a graphical tool to explore the variability of a functional data set

Finally, the last step of our analysis is to explore the variability of a set of individual space-speed profiles. Indeed, if the construction of an aggregated speed profile, such as the average profile, leads to a good representation of the actual speeds on a road network section, such an aggregated profile does not reflect the variability between road users. The boxplot proposed by Tukey (1977) is a graphical method used to represent the distribution of univariate data, and can be used to represent speed variations between individuals at a given point. For example, Fig. 9.a represents pointwise boxplots calculated at a regular interval of 10 m in the red light case, with medians connected by a red line (V50 profile) and 85th percentiles connected by a blue line (V85 profile). However, this representation lost the continuous form of the individual profiles, and then the V50 and V85 profiles are not true space-speed profiles as defined in Definition 1 in contrast to the average speed profile obtained at Fig. 8.b.

So, we propose to use a graphical tool called functional boxplots, recently developed by Sun and Genton (2011), which extends the notion of boxplots to functional data. This tool is based on the notion of functional depth which generalizes order statistics or ranks to the functional setting. Indeed, the first step to construct a boxplot is the data ordering. But if the notion of order is obvious in the univariate setting, it is much more complicated in the functional setting. This problem has led to the emergence of the concept of functional depth, first introduced for multivariate data (Zuo and Serfling 2000), that provides a measure of "centrality" and "outlyingness" for a function within a sample of curves and allows to order them from center-outward (López-Pintado and Romo 2009). The median curve is then the curve with the higher depth. Various examples of functional depth have been proposed in the literature such as the Fraiman and Muniz depth (Fraiman and Muniz 2001), the random projection depth (Cuevas et al 2007) or the band depth (López-Pintado and Romo 2009). If Sun and Genton (2011) use the band depth and its modified version for the construction of its functional boxplots, a comparison of the results obtained with various functional depth led us to choose the h-mode

depth introduced by Cuevas et al (2006) and based on the concept of mode. The authors defined a functional mode as the curve most densely surrounded by the rest of curves of the dataset. Thus, the h-modal functional depth of a curve x_i with respect the set of curves $x_1, \ldots, x_n$ is given by:

$$MD_n(x_i, h) = \sum_{k=1}^{n} K(\frac{\|x_i - x_k\|}{h}), \tag{18}$$

where $\|.\|$ is an appropriate norm, K is a kernel function, and h is a bandwidth. In practice, the L^2 norm and the truncated Gaussian kernel are used, and the bandwidth taken is the 15th percentile of the empirical distribution of $\{\|x_i - x_k\|,\ i, k = 1, \ldots, n\}$. Functional boxplots create with the h-modal depth are illustrated in Fig. 9.b in the red light case. This functional boxplot is composed of the maximum enveloppe (blue curves), the median profile (black curve) which is the most central curve with the highest h-modal depth, the 25% central region (dark magenta region), the 50% central region (magenta region) and the 75% central region (pink region). The red dashed curves are the outlier candidates detected by the 1.5 times the 50% central region rule (see Sun and Genton 2011). This functional boxplot have been computed with the function `fdepth` of the R package `rainbow` and the function `fbplot` of the R package `fda`.

The advantage of this graphical tool is that it allows to represent the speed dispersion among individuals on a given road section. These speed corridors allow to distinguish road sections where the speed variability is large and those for which speeds are more homogeneous. Moreover, this tool leads to the extraction of the median profile which depends to the choice of a functional depth, and that can be used as a representative speed profile of the set of the individual speed profiles instead of the average profile.

7 Conclusion

In this paper, we have proposed a functional analysis of a set of space-speed profiles corresponding to speed as function of the distance traveled by the vehicle from an initial point. Thus, a definition of the functional space of these objects was proposed and the study of their mathematical properties has shown the remarkable property of non differentiability at points for which speed is zero and that corresponds to a cusp in the curve. Then, the first step of our analysis was the development of a smoothing procedure in order to be reduced to a functional framework. However, we have shown that the estimation of a space-speed profiles from noisy position and speed measurements was complex and can be reduced to a nonparametric regression problem taking into account two constraints: the use of the derivative information, and a monotonicity constraint. A two-step estimator (smooth, and then monotonize) based on the

a. Pointwise boxplots.

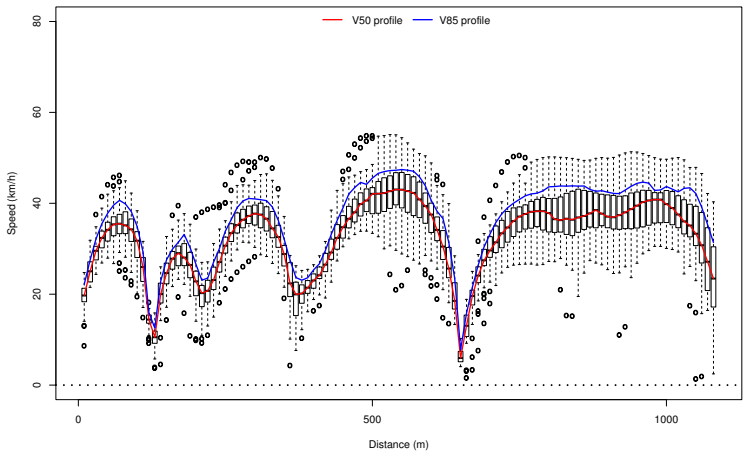

b. Functional boxplots.

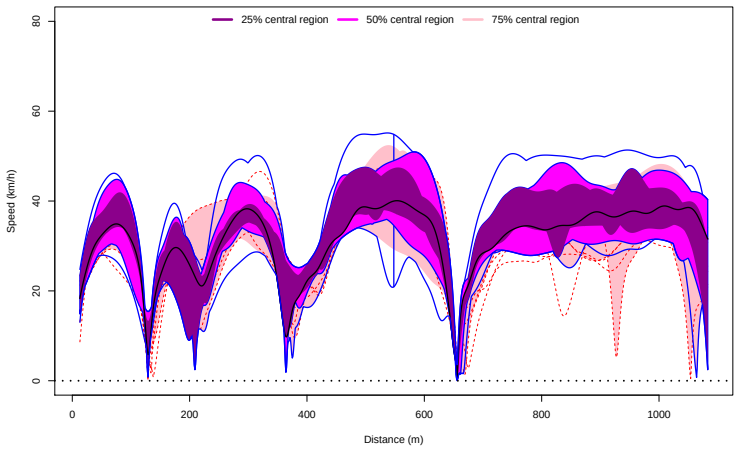

Fig. 9 Pointwise boxplots ans functional boxplots in the red light case (36 curves).

general theory of thin-plate spline was proposed and computed on simulation studies and on a real data set. If the proposed smoothing procedure presents good results, some limitations appear in the estimation of points for which the function is zero (speed tends to be overestimated at short stops). This point is an important challenge for the future, and the fusion of the two constraints in a single smoothing step will be subject to future research.

In a second time, a methodology has been proposed to summarize a set of individual space-speed profiles with an aggregated speed profile. The functional approach allows to use curve registration method in order to correct

phase variation, and then to obtain a representative average speed profile with similar features of corresponding individual speed profiles. The method of landmarks alignment, which consists to align specific points of the curves, is applied on a data set where two driving situations corresponding to the state of the traffic light (red or green light) are distinguish. A comparison of the unregistered and the registered speed profiles at stops imposed by the infrastructure in the red light case, as well as the corresponding average profiles, illustrates the interest of the method. The development of unsupervised classification methods to distinguish traffic conditions (free vs congestion) or specific driving conditions (state of traffic lights) could also be subject to future works.

Finally, the variability of a set of individual space-speed profiles was explored by the use of functional boxplots, initially proposed by Sun and Genton (2011), which are an extension of the classical boxplots used in the univariate setting. This tool leads to the construction of speed corridors that reflect the variability between road users.

Acknowledgements The authors would like to gratefully thank Christine Thomas-Agnan from the University of Toulouse I for discussions about RKHS and the general smoothing problem, and for her help in the use of the derivative information in the smoothing procedure presented in this article. We thank Yuedong Wang from the University of California for his help in the implementation of the smoothing procedure with the R package `assist`, and Jeremie Bigot from the Toulouse Mathematics Institute for discussions about the present study. This work was funded by the French Institute of Science and Technology for Transport, Development and Networks (IFSTTAR).

A Proofs of properties given in Section 3.2

Proof of Theorem 1:
Let $x_0 \in [0, x_f]$. There are two distinct cases :
1st case : x_0 is a point of continuity of F^{-1}. Then by composition of two continuous functions, we deduce that $F' \circ F^{-1}$ is continuous at x_0.
2nd case : x_0 is a point of discontinuity of F^{-1}. We begin by demonstrating the following lemma:

Lemma 1 *Let $x_0 \in [0, x_f]$ a point of discontinuity of F^{-1}. Then the speed is zero at this point, i.e. $v_S(x_0) = F' \circ F^{-1}(x_0) = 0$.*

This lemma can be proved easily. Indeed, if x_0 is a point of discontinuity of F^{-1}, then there is a close interval $[t^-, t^+]$ where F is constant and equal to x_0, and by definition of F^{-1}, $F^{-1}(x_0) = t^-$. This implies that $F'_+(t^-) = 0$ where $F'_+(t^-)$ is the right derivative of F at t^-, and as it was assumed that F was differentiable, we also have $F'_-(t^-) = 0$ where $F'_-(t^-)$ is the left derivative of F at t^-. Finally, $F'(t^-) = 0$, and therefore $F' \circ F^{-1}(x_0) = 0$ which ends the proof of the lemma 1.
Now, we study the one-sided limit of $v_S = F' \circ F^{-1}$ at x_0. $(v_S)_-(x_0) = \lim\limits_{\substack{x \to x_0 \\ x < x_0}} v_S(x) = \lim\limits_{\substack{x \to x_0 \\ x < x_0}} F' \circ F^{-1}(x)$. When $x \to x_0$ by lower values, $t \to t^-$ by lower values, and $\lim\limits_{\substack{t \to t^- \\ t < t^-}} F'(t) = 0$ since $F'(t) = 0$ on $[t^-, t^+]$ and F' is continuous at t^-. So, we deduce that $(v_S)_-(x_0) = 0$.

Similarly, $(v_S)_+(x_0) = \lim\limits_{\substack{x\to x_0\\ x>x_0}} v_S(x) = \lim\limits_{\substack{x\to x_0\\ x>x_0}} F' \circ F^{-1}(x)$. When $x \to x_0$ by upper values, $t \to t^-$ by upper values, and $\lim\limits_{\substack{t\to t^-\\ t>t^-}} F'(t) = 0$ since $F'(t) = 0$ on $[t^-, t^+]$. So, we deduce that $(v_S)_+(x_0) = 0$. Hence, using Lemma 1, we conclude that v_S is continuous at x_0. □

Proof of Theorem 2:

1st case: Assume that F satisfies the assumptions (H_1).
Let x_0 such that $t_0 = F^{-1}(x_0)$. Since $F'(t_0) = 0$, then $v_S(x_0) = 0$, i.e. $x_0 \in H_0$. Under the assumptions (H_1), we can apply the Taylor-Young's formula to F': For all θ in a neighborhood of t_0, $F'(t_0+\theta) = F'(t_0)+\theta F''(t_0)+\frac{\theta^2}{2}F'''(t_0)+\theta^2\varepsilon(\theta)$, where $\varepsilon(\theta) \to 0$ when $\theta \to 0$. But since $F'(t_0) = 0$, if we had $F''(t_0) \neq 0$, then F' would change sign at t_0, which contradicts the strict monotonicity of F. Therefore $F''(t_0) = 0$. So, $F'(t_0 + \theta) \underset{\theta\to 0}{\sim} \frac{\theta^2}{2}F'''(t_0)$ (since it is assumed that $F'''(t_0) \neq 0$).
Let $h = F(t_0 + \theta) - F(t_0)$. We apply the Taylor-Young's formula to F :
$h = F(t_0 + \theta) - F(t_0) = \theta F'(t_0) + \frac{\theta^2}{2}F''(t_0) + \frac{\theta^3}{6}F'''(t_0) + \theta^3\varepsilon'(\theta)$ where $\varepsilon'(\theta) \to 0$ when $\theta \to 0$. In order to study the differentiability of v_s at x_0, we define the following growth rates:
$\frac{v_S(x_0+h)-v_S(x_0)}{h} = \frac{F'(t_0+\theta)-F'(t_0)}{F(t_0+\theta)-F(t_0)} \underset{\theta\to 0}{\sim} \frac{\frac{\theta^2}{2}F'''(t_0)}{\frac{\theta^3}{6}F'''(t_0)} = \frac{3}{\theta}$. This growth rate has no limit when $\theta \to 0$, but this does not prove that it has also no limit when $h \to 0$.
We will prove this by contradiction. Assume that $\frac{v_S(x_0+h)-v_S(x_0)}{h} \underset{h\to 0}{\to} \ell \in \mathbb{R}$. Then, by definition,
$\forall\varepsilon > 0$, $\exists\alpha > 0$ such that $|h| < \alpha \Rightarrow |\frac{v_S(x_0+h)-v_S(x_0)}{h} - \ell| < \varepsilon$.
But since F is continuous at t_0, $\exists\beta > 0$ such that $|t - t_0| < \beta \Rightarrow |F(t) - F(t_0)| < \alpha$, or similarly $|\theta| < \beta \Rightarrow |\underbrace{F(t_0 + \theta) - F(t_0)}_{h}| < \alpha$.
Hence, $\forall\varepsilon > 0$, $\exists\beta > 0$ such that $|\theta| < \beta \Rightarrow |\frac{v_S(x_0+h)-v_S(x_0)}{h} - \ell| < \varepsilon$. This means that the growth rate has a limit $\ell \in \mathbb{R}$ when $\theta \to 0$, which is a contradiction. Hence, under the assumptions (H_1), v_S is not differentiable at x_0.

2nd case: Assume that F satisfies the assumptions (H_2).
As in the first case, we define x_0 such that $t_0 = F^{-1}(x_0)$. The graph of G :

- coincides with F on $[0, t_0]$,
- is deduced from the graph of F by the translation vector $(t_0 - t_1)\overrightarrow{i}$ on $[t_0, T-(t_1-t_0)]$.

Thus, the graph of G is similar to the graph of F but removing the time period $[t_0, t_1]$ for which the function is constant. So, the same growth rate occurs at x_0, and if v_S is not differentiable at x_0 for one, it is not for the other. In other words, the results of the first case where $F' = 0$ at one point t_0 extend to the more general case where F' is zero on an interval $[t_0, t_1]$ $(t_0 \neq t_1)$, subject to the assumptions (H_1) on G. □

References

Andrieu C (2013) Modélisation fonctionnelle de profils de vitesse en lien avec l'infrastructure et méthodologie de construction d'un profil agrégé. PhD thesis, Université Toulouse 3 Paul Sabatier

Andrieu C, Saint Pierre G, Bressaud X (2012) Modélisation fonctionnelle et lissage sous contraintes d'un profil spatial de vitesse. In: 44ème Journées de Statistique, Bruxelles, Belgique

Andrieu C, Saint Pierre G, Bressaud X (2013) Estimation of space-speed profiles: A functional approach using smoothing splines. In: Proceedings of the IEEE Intelligent Vehicle Symposium (IV 2013), Gold Coast, Australie, juin 2013

Berlinet A, Thomas-Agnan C (2004) Reproducing kernel Hilbert spaces in probability and statistics, vol 3. Kluwer Academic Boston

Bigot J (2006) Landmark-based registration of curves via the continuous wavelet transform. J Comput Graph Stat 15(3):542–564

Bigot J, Gadat S (2010) Smoothing under diffeomorphic constraints with homeomorphic splines. SIAM Journal on Numerical Analysis 48(1):224–243

Brunk HD (1955) Maximum likelihood estimates of monotone parameters. Ann Math Stat 26:607–616

Calderon C, Martinez J, Carroll R, Sorensen D (2010) P-splines using derivative information. Multiscale Modeling and Simulation 8(4):1562–1580

Cox D (1988) Approximation of method of regularization estimators. Ann Stat pp 694–712

Cuevas A (2013) A partial overview of the theory of statistics with functional data. J Stat Plan Inference

Cuevas A, Febrero M, Fraiman R (2006) On the use of the bootstrap for estimating functions with functional data. Comput Stat Data Anal 51(2):1063–1074

Cuevas A, Febrero M, Fraiman R (2007) Robust estimation and classification for functional data via projection-based depth notions. Comput Stat 22(3):481–496

Delecroix M, Thomas-Agnan C (2000) Spline and kernel regression under shape restrictions. In: Smoothing and Regression: Approaches, Computation, and Application, Wiley, New York, pp 109–133

Delecroix M, Simioni M, Thomas-Agnan C (1996) Functional estimation under shape constraints. J Nonparametric Stat 6(1):69–89

Duchon J (1977) Splines minimizing rotation-invariant semi-norms in sobolev spaces. In: Constructive theory of functions of several variables, Springer-Verlag, Berlin, pp 85–100

Febrero M, Galeano P, González-Manteiga W (2007) A functional analysis of nox levels: location and scale estimation and outlier detection. Comput Stat 22(3):411–427

Ferraty F, Vieu P (2006) Nonparametric Functional Data Analysis: Theory and Practice. Springer Series in Statistics, Springer, New York

Fraiman R, Muniz G (2001) Trimmed means for functional data. Test 10(2):419–440

Gu C (2002) Smoothing spline ANOVA models. Springer, New York

Hall P, Yatchew A (2007) Nonparametric estimation when data on derivatives are available. Ann Stat 35(1):300–323

Kneip A, Gasser T (1992) Statistical tools to analyze data representing a sample of curves. Ann Stat pp 1266–1305

Levitin DJ, Nuzzo RL, Vines BW, Ramsay JO (2007) Introduction to functional data analysis. Canadian Psychology 48(3):135–155

López-Pintado S, Romo J (2009) On the concept of depth for functional data. J Am Stat Assoc 104(486):718–734

Mammen E, Marron J, Turlach B, Wand M (2001) A general projection framework for constrained smoothing. Statist Sci pp 232–248

Mardia K, Kent J, Goodall C, Little J (1996) Kriging and splines with derivative information. Biometrika 83(1):207–221

Meinguet J (1979) Multivariate interpolation at arbitrary points made simple. Zeitschrift für angewandte Mathematik und Physik ZAMP 30(2):292–304

R Core Team (2013) R: A Language and Environment for Statistical Computing. R Foundation for Statistical Computing, Vienna, Austria, URL http://www.R-project.org/

Ramsay J (1988) Monotone regression splines in action. Statist Sci pp 425–441

Ramsay J (1998) Estimating smooth monotone functions. J R Stat Soc B 60(2):365–375

Ramsay J, Li X (1998) Curve registration. J R Stat Soc B 60(2):351–363

Ramsay JO, Silverman BW (2002) Applied Functional Data Analysis: Methods and Case Studies. Springer Series in Statistics, Springer, New York

Ramsay JO, Silverman BW (2005) Functional Data Analysis, Second Edition. Springer, New York

Sun Y, Genton M (2011) Functional boxplots. J Comput Graph Stat 20(2)

Tukey J (1977) Exploratory data analysis. Reading, MA 231

Valderrama MJ (2007) An overview to modelling functional data. Comput Stat 22(3):331–334

Wahba G (1990) Spline models for observational data. SIAM, Philadelphia PA

Wahba G, Wendelberger J (1980) Some new mathematical methods for variational objective analysis using splines and cross-validation. Mon Weather Rev 108:1122–1145

Wang K, Gasser T (1997) Alignment of curves by dynamic time warping. Ann Stat 25(3):1251–1276

Wang Y (2011) Smoothing Splines: Methods and Applications. Monographs on Statistics and Applied Probability, Taylor & Francis US

Wang Y, Ke C (2004) Assist: A suite of s functions implementing spline smoothing techniques. University of California, Santa Barbara

Zuo Y, Serfling R (2000) General notions of statistical depth function. Ann Stat pp 461–482